Generation and 355 nm Laser Photodissociation of Nitrous Acid (HONO) and HONO−Water Clusters

C. L. Ning and J. Pfab*

Department of Chemistry, Heriot-Watt University, Riccarton, Edinburgh, EH14 4AS, Scotland, U.K.

Received: April 3, 1997; In Final Form: June 10, 1997[⊗]

A stable source for the continuous production of high concentrations of gaseous nitrous acid (HONO) up to 5000 ppm has been developed, characterized, and employed for a study of the near-UV photodissociation of HONO and HONO−water clusters in a continuous supersonic free-jet expansion. The source consists of a flow reactor fed with aqueous reagent solutions purged by an inert carrier gas at flow rates up to 1 L/min. The dynamics of the photodissociation of jet-cooled HONO and HONO−water clusters at 355 nm have been studied by measuring the rotational distribution of the nascent NO ($v'' = 2$) photofragment using the laser-induced fluorescence (LIF) technique. Distinctly bimodal rotational distributions have been observed for the nascent, vibrationally excited NO, which are well described by the sum of two components: a Gaussian distribution at high *J* and a 170 K Boltzmann distribution in the low-*J* range reflecting photodissociation of bare HONO , HONO−H_2O complexes, and small HONO water clusters.

Introduction

The photodissociation of nitrous acid in the near-UV makes a major contribution to the production of hydroxyl radicals in sunlit air masses and significantly influences the daytime chemistry of the atmosphere.[1] Nitrous acid has also been observed as an indoor air pollutant, and there is much current interest in its heterogeneous and aerosol chemistry.[2] The transition from bare, isolated HONO molecules to HONO−water aerosols and the accompanying changes in the dynamics of its photodissociation to hydroxyl radicals and nitric oxide (eq 1) are of fundamental interest and also directly relevant in atmospheric chemistry:

$$\mathrm{HO{-}N{=}O}(\tilde{X}^1A') + h\nu \rightarrow \mathrm{HO{-}N{=}O}(\tilde{A}^1A'') \rightarrow \mathrm{HO}(X\,^2\Pi) + \mathrm{NO}(X^2\Pi) \quad (1)$$

Studies of photodissociation processes of molecular clusters have recently developed into a rapidly growing field, since they offer the prospect of achieving a better, microscopically detailed understanding of the dynamics of elementary reactions in the condensed phase. Recent experiments on cluster photochemistry have exploited the power of pulsed laser dissociation−probe techniques to map the partitioning of excess energy into translational and internal degrees of freedom of nascent atoms or diatomic photofragments, respectively. Measurements of the distribution of energy and momenta partitioned into small fragments, such as H, O, OH, or I_2, can provide information about their parentage and can yield dynamical information about their formation and the relaxation of the excess energy in weakly bonded clusters.[3−6]

The photodissociation of bare nitrous acid has been studied by several groups at different photolysis wavelengths, and both OH and NO photofragments have been probed by state-resolved laser-induced fluorescence (LIF) spectroscopy,[7−12] yielding information on the scalar and vector attributes of both fragments and the dynamics of the dissociation from the $S_1(n,\pi^*)$ state. In contrast little effort appears to have been made to characterize the photodissociation of HONO clusters, although the effects of unwanted clustering have been observed.[8,10,11] The poor stability of HONO toward thermal and surface-catalyzed decomposition and the experimental difficulties involved in generating high concentrations of this compound in the absence of water, nitrogen oxides (NO_x, N_2O), and nitric acid[7,8,12] may have discouraged attempts to study the clusters of nitrous acid.

Gas-phase samples of HONO can be prepared by the reaction of aqueous sodium nitrite with dilute sulfuric acid at 273 K (eq 2) and evaporation of the resulting solution. Cox and co-workers have shown that vapor-phase HONO concentrations greater than those involved in the thermodynamic equilibrium among NO, NO_2, and water vapor can be obtained in this way:[13,14]

$$2\mathrm{NaNO_2} + \mathrm{H_2SO_4} \rightarrow 2\mathrm{HONO} + \mathrm{Na_2SO_4} \quad (2)$$

Storing the gaseous products of this reaction in a cooled reservoir preserves high nonequilibrium concentrations of HONO. Typical HONO mixing ratios generated in this way are of the order of 200 ppm. Similar batch preparative methods have been described[12,15,16] and can be adapted with suitable modifications to produce pulsed molecular beams. Difficulties experienced in controlling fluctuations in the sample stagnation pressure when employing the discontinuous technique provided an incentive to develop a continuous method. Continuous jets can provide good sample stability and can be used in conjunction with simple, corrosion resistant glass nozzles but demand a sample source capable of supplying higher concentration. For photodissociation studies of HONO in a continuous jet we aimed at volume mixing ratios on the order of 1% prior to expansion corresponding to 1×10^4 ppm HONO.

Taira and Kanda have previously described a continuous source of nitrous acid for the concentration around 1 ppm,[17] employing solutions of sodium nitrite and sulfuric acid mixed and purged continuously with a carrier gas. More recently Febo et al. have demonstrated that the reaction of gaseous HCl with solid $NaNO_2$ can generate very pure HONO at mixing ratios up to 20 ppm.[1] Gaseous oxalic acid subliming into solid $NaNO_2$ has also been used to generate HONO at very low concentration in air.[18] These sources provide HONO vapor with little contamination by NO_x and HNO_3 but cannot be employed for generating higher concentration levels . One aim of the present work was therefore to develop and characterize a source of high

[⊗] Abstract published in *Advance ACS Abstracts,* July 15, 1997.

S1089-5639(97)01171-7 CCC: $14.00

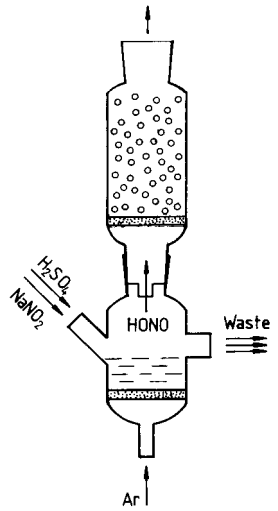

Figure 1. Schematic of the glass reaction vessel used for the generation of HONO.

HONO concentrations. Another objective was to study the photodissociation of bare HONO and of HONO−water clusters in a continuous free-jet expansion.

In the present work we describe a flow-type reactor based on reaction 2, which provides a stable, continuous supply of high concentrations of gaseous HONO. We demonstrate that this source is suitable for the production of HONO−water clusters in a continuous supersonic free-jet expansion. The application of this source is described for the 355 nm photodissociation of jet-cooled HONO and HONO−water clusters, employing the technique of pulsed laser photolysis (PLP) with laser-induced fluorescence (LIF) probing of the nascent NO.

Experimental Section

Nitrous Acid Generator. Figure 1 shows the schematic of the glass reactor employed for the generation of gaseous HONO by the reaction of aqueous sodium nitrite and sulfuric acid solutions. The 200 mm long glass vessel was cylindrical and consisted of two compartments of 4 cm diameter separated by a coarse frit, a glass constrictor with a central orifice of 5 mm diameter, and a standard B19/26 ground glass joint. The chemical reaction of the aqueous reagent solutions took place in the lower compartment. The upper compartment above the frit was filled with broken glass and glass beads of 2 mm diameter serving as a demister to remove coarse droplets from the spray entrained by the carrier gas. The top of the vessel was connected to glass tubing via a standard B19/26 ground glass joint. The bottom compartment of the reactor was immersed in a water bath permitting variation of the temperature between 0 and 50 °C. Aqueous sodium nitrite and sulfuric acid solutions were pumped separately into the lower chamber by a peristaltic pump. The reaction mixture is agitated vigorously by purging with a rapid stream of the carrier gas through a frit of porosity 2. Three channels of the peristaltic pump were used to remove the reactor waste. By control of the feed and waste pumping speeds, it was possible to maintain the volume of the reaction mixture constant at about 25 mL.

Gaseous products together with water vapor are entrained by the rare gas that is supplied via a needle valve to the inlet at the bottom of the lower chamber. After passing through the bubble breaker and demister sections of the vessel, the gas mixture was fed through glass and PVC connecting tubing to the supersonic jet source. Gas consumption by the jet was limited by the nozzle orifice and the throughput of the pumping system. Control of the stagnation pressure was provided by a metering valve in the supply line in conjunction with an MKS baratron capacitance gauge, a flow meter, and a glass−Teflon valve on the sample supply side. A bypass to waste via a caustic soda scrubber permitted venting of excess gas to a fume hood.

Absolute concentrations of HONO and NO_2 were measured with a UV spectrophotometer (Shimadzu UV-240) using a fused silica cell of 10 cm path length under flow conditions. The pressure in the cell was monitored by a Baratron gauge and kept at 820 Torr.

Free-Jet Expansion, Photolysis, and LIF Analysis. For jet-cooling of HONO and for the generation of its clusters, the carrier gas seeded with HONO was connected to a 30 cm length of Pyrex glass tubing, the end of which was formed into a nozzle with a smooth circular 0.2 mm diameter hole. A range of different orifice sizes from 0.1 to 0.5 mm were used in initial measurements. The supersonic free-jet expansion was formed by mounting the nozzle vertically on the top flange of a vacuum chamber. The nozzle could be moved vertically through a sliding, "O"-ring-sealed shaft and horizontally by motion in the *xy* plane using micrometer-driven sliding motion of a small lubricated, floating "O"-ring-sealed flange against the stationary main flange. The vacuum chamber was made of black anodized aluminum of construction similar to that described elsewhere.[19,20] It was evacuated to a base pressure of 10^{-4} Torr via a liquid-nitrogen-cooled, removable stainless steel trap by a high-capacity booster (Edwards EH250) in combination with a mechanical rotary pump (Edwards E2M80). The purpose of the cold trap was to reduce the contamination of the pumps by the corrosive acids and nitrogen oxides. During free-jet expansion at a stagnation pressure of 820 Torr a background pressure of 9×10^{-2} Torr was measured with the 150 μm diameter nozzle and with Ar as the carrier gas. These conditions were used for all measurements reported in the Results section unless specified otherwise. Under these conditions the rotational temperature of the cold NO in the central portion of the jet 5−6 mm downstream of the orifice, which formed the observation volume imaged by the detector, was measured to be around 10 K by LIF on the (0,0) band of the $A^2\Sigma^+ \leftarrow X^2\Pi_{1/2}$ transition near 225 nm. Previous measurements using LIF in the red region of the spectrum have shown that the rotational cooling of NO_2 in supersonic jets of Ar is only marginally less than that for NO.[19,20] This leads us to conclude that the rotational temperature of the HONO achieved by jet-cooling with Ar is also in the range 10−20 K under the conditions used. All results reported were obtained with a 150 μm diameter nozzle and with Ar as the carrier gas. Experiments conducted with He as the carrier gas were attempted, but the LIF excitation spectra of NO($v = 1$ and 2) indicated that jet-cooling of NO and NO_2 was too inefficient under these conditions, leading to unacceptable interference in the NO($v = 2$) photofragment spectra.

The basic arrangement of the experimental setup used was very similar to that reported elsewhere[20] and consisted of a conventional coaxial pump−probe beam configuration with both photolysis and probe pulses derived from the same Q-switched Nd:YAG laser. The typical output of 30 mJ of the third harmonic of the YAG laser (Lumonics HY400) operating at 10 Hz repetition rate was split into two beams of which 5 mJ was used for photolysis and the remainder of 25 mJ was employed as the pump radiation for a coumarin dye laser (Lumonics HD500) with a nominal bandwidth of 0.15 cm^{-1}. The 472 nm output of the dye laser was frequency doubled with a customary second harmonic generation unit (Lumonics Hyper Trak-1000) and produced the required probe radiation for interrrogating the nascent NO photofragment on the (0,1) and (0,2) bands of the $A \leftarrow X$ transition near 236 and 245 nm, respectively. The probe

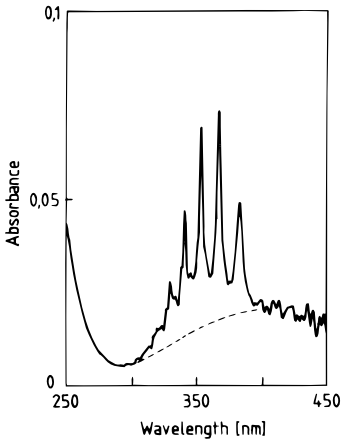

Figure 2. Electronic absorption spectrum of the gaseous products of the HONO reactor under the following experimental conditions: $NaNO_2$ and H_2SO_4, 2 mol/L; pump rate, 4 mL/min; gas flow rate, 0.4 L/min; temperature, 20 °C. The dashed line is the absorbance of NO_2 redrawn to scale from ref 32.

pulses were optically delayed by 8 ns with respect to the 5 ns long photolysis pulses.

The counterpropagating pump and probe beams were polarized vertically, aligned coaxially, and intersected the supersonic jet at a distance of about 6 mm downstream from the orifice. The laser-induced fluorescence of the NO photofragment was imaged by a fused silica condensor onto a photomultiplier. A gated integrator and boxcar averager was used to process the PMT signal. Signals were digitized and stored in a laboratory computer. Other details of the LIF detection and signal acquisition have been described previously.[20] Note that conditions of optical saturation of the A ← X transition had to be used to obtain sufficient NO(v=2) signal. The main factor limiting the signal-to-noise ratio was laser light scattered by the jet.

Results

Evaluation of HONO Generator. Most of the measurements were conducted with Ar as the inert gas, since jet-cooling with He was found to be less efficient leading to interference. Volatile components expected in the carrier gas on exiting the HONO generator are H_2O, HONO, NO, and NO_2 apart from HNO_3, N_2O, and very small amounts of N_2O_4 and N_2O_3 . HNO_3 and N_2O cannot interfere in any of the subsequent measurements, and the thermal equilibria disfavor N_2O_3 and N_2O_4 at 293 K. To quantify the products absorbing at 355 nm, the electronic absorption spectra of the gas mixture were measured under typical operational conditions: concentration and pump rate of reagents, 2 mol L^{-1} at 4 mL min^{-1}; gas pressure and temperature, 820 Torr and 293 K; Ar flow rate, 0.4 L min^{-1}.

The solid line in Figure 2 displays the absorption spectrum of the product gas in the range 250−450 nm under the typical conditions used and shows the progression in the excited-state N═O stretching vibration characteristic of the A ← X electronic transition of HONO on top of the NO_2 absorption. The HONO contribution to the total absorbance could be estimated by subtracting the contribution of NO_2. Absorption cross sections of HONO at 300 and 400 nm are negligible compared to NO_2 but amount to 5.2×10^{-19} cm^2 at the absorption maximum near 370 nm.[16] Calculated volume mixing ratios of NO_2 and HONO are 160 and 820 ppm for the example shown. The calculated NO_2 contribution is shown by the dashed line in Figure 2. Partial pressures of NO were estimated from the absorbances of the γ(0,0) and γ(1,0) bands near 225 and 235 nm, respectively, after dilution with the carrier gas.

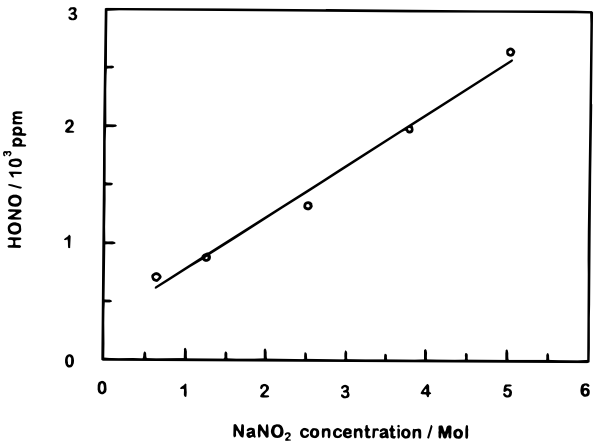

Figure 3. HONO production as a function of the concentration of the $NaNO_2$ solution for $[H_2SO_4] = 5$ mol/L.

HONO yields in the seeded carrier gas were monitored routinely via the NO($v = 2$) photofragment LIF signal obtained from the free-jet expansion. The LIF signal $I_{J'J''}$ for a particular rovibronic transition of the photofragment depends on many parameters in addition to those arising from the sample generation. Some of the factors including the intensities I_{ph} and I_{pr} of the photolysis and probe laser pulses important in the experiment are summarized by the following equation:

$$[\mathrm{HONO}] \propto [\mathrm{NO}(v = 2)] \propto I_{J'J''} \propto \eta\rho\delta I_{ph} I_{pr} \qquad (3)$$

Here η stands for the fractional yield of nascent NO occupying the probed rovibronic ground-state level and ρ for a geometry factor that takes into account the degree of overlap between the photolysis, probe, and fluorescence observation volumes. δ is a similar factor that depends on the position of this effective sampling volume in the jet expansion and on the size of the nozzle orifice. In practice the dependence on I_{pr} was minimized by employing saturated LIF for NO.

Relative LIF measurements were converted to HONO mixing ratios employing the UV absorption measurements of the 293 K gas mixture for calibration. The yield of HONO was found to depend on several factors: the concentrations of the reagent solution, their pump rate, the temperature of the reaction mixture, and the flow rate of Ar. To optimize the method, it was necessary to measure the dependence of the HONO output on each factor separately while the other parameters were kept constant. The concentration of the reagent solutions was found to dominate the HONO output of the reactor. Figure 3 shows the dependence of the HONO output on the concentration of the $NaNO_2$ solution for $[H_2SO_4] = 5$ mol L^{-1} with the other conditions typical as defined previously. Clearly, the number density of HONO entrained into the Ar carrier gas increases linearly with $[NaNO_2]$ with a slope of 500 ppm mol^{-1} L up to the highest nitrite concentration used (5 mol L^{-1}), yielding an HONO volume mixing ratio of 2700 ppm.

The dependence of the HONO yield on the pump rate of the reagent solutions in the range 1.5−14 mL/min is plotted in Figure 4 for reactant concentrations of 2 mol L^{-1} and a reactor temperature of 20 °C. A linear dependence with a small slope is seen such that an increase in the pump rate from 4 to 14 mL/min merely increases the HONO yield from 800 to 1400 ppm. A low reagent pump rate of 4 mL/min was therefore used under the typical conditions described previously in the Experimental Section.

The reaction temperature was found to exert a minor influence on the HONO yield as shown clearly in Figure 5 with the HONO output remaining almost constant at temperatures higher than

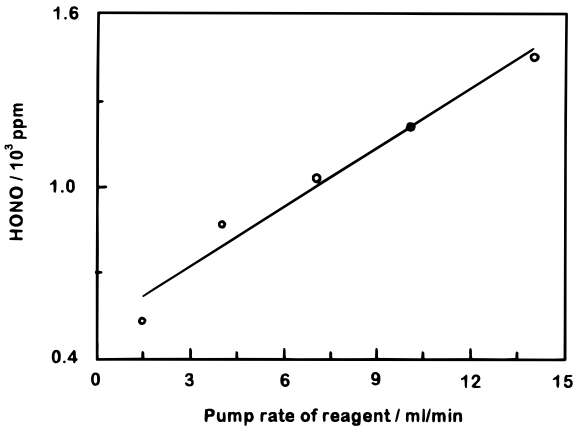

Figure 4. Effect of reagent pump rate on the HONO output of the reactor measured at a total pressure of 820 Torr.

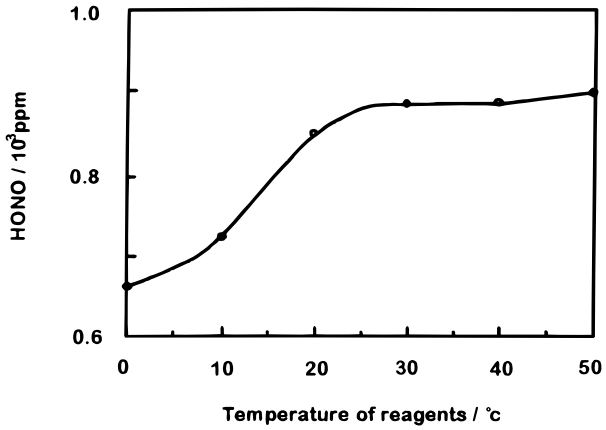

Figure 5. HONO output at different temperature of the reagent solution under standard conditions defined in the text.

20 °C and dropping slightly for lower temperatures. Since the water vapor density will increase exponentially with the reactor temperature while HONO yields remain nearly constant, the photodissociation experiments were conducted at a reactor temperature of 20 °C.

The stability of the HONO generation method was also tested by monitoring HONO yields with the flow cell and spectrophotometer under the typical operating conditions described above with the reactor running at an HONO output level of 800 ppm. Over a 2 h period the HONO output was found to vary less than 15%.

The main chemical species entrained by the carrier gas are H_2O, HONO, and small amounts of NO and NO_2. The concentrations of NO and NO_2 are too small for significant dimer and N_2O_3 formation at the pre-expansion temperature of 293 K.[14] We also neglect N_2O and HNO_3 that may be formed as very minor side products.[21] The measurements described and a crude estimate of the water vapor pressure under the typical operating conditions indicate that the main constituents of the gas mixture prior to expansion occur in the proportion

$$\mathrm{Ar(He)}:\mathrm{H_2O}:\mathrm{HONO}:\mathrm{NO}:\mathrm{NO_2} = 800:18:0.68:0.14:0.14 \quad (4)$$

HONO and Cluster Photolysis. The 355 nm photodissociation of HONO was studied under the typical conditions described previously with a total gas flow rate for HONO production of 0.4 L/min. All results reported refer to Ar as the carrier gas. We first consider interference from NO_2, N_2O_3, and N_2O_4. The photodissociation of NO_2, which occurs as an unavoidable, significant component in the expansion, also leads to nascent NO, and care needs to be taken to exclude its interference. The excess available energy released by 355 nm photodissociation of cold NO_2 is sufficient to populate the NO in the $v'' = 0$ and $v'' = 1$ levels but fails to produce any NO($v'' = 2$).[20,22] Any interference from the one-photon dissociation of cold NO_2 according to eq 5 is therefore minimized by confining measurements to NO in its $v'' = 2$ level and by avoiding conditions favoring the multiphoton dissociation of NO_2:

$$\mathrm{NO_2} + h\nu\ (355\ \mathrm{nm}) \rightarrow \mathrm{NO}(v'' = 0, 1) + \mathrm{O}(^3\mathrm{P_J}) \quad (5)$$

The photodissociation of jet-cooled N_2O_3 might also lead to interference, since it has a measurable electronic absorption in the near-UV and a weakly bound nitroso (N═O) group.[23] Experiments conducted with a sample of 5 Torr of an equimolar mixture of NO and NO_2 expanded with Ar under otherwise typical conditions only gave rise to a very small LIF signal for NO($v'' = 2$) comparable to that from pure, expansion-cooled NO_2. We are therefore led to conclude that N_2O_3 photolysis does not interfere significantly. NO($v'' = 2$) formation in samples rich in NO_x appears to arise from two- or multiphoton dissociation of NO_2 by the 355 nm laser pulses, which exhibit the unavoidable temporal and spatial fluctuations characteristic of a Q-switched solid-state laser. This was confirmed by separate experiments employing a larger fraction of the 355 nm pump laser output for photolysis and by focusing the photolysis beam. Such unfavorable conditions led to substantial LIF signals for NO($v'' = 2$) and were therefore avoided. Use of He instead of Ar also led to significant interference that we attribute to rotationally hot NO($v'' = 1$) and additional NO($v'' = 2$) from the photodissociation of warm NO_2. This interference precluded the use of He for jet-cooling.

Any NO($v'' = 2$) contribution from the symmetric dimer N_2O_4 will also be slight because of its small abundance, modest absorption at 355 nm, and zero predicted quantum yield for one-photon dissociation to NO($v'' = 2$). N_2O_3 also absorbs at 355 nm via a continuous $S_2 \leftarrow S_0$ electronic transition.[23] In alkyl nitrites (RO−N═O), nitrosamines (R_2N−N═O), and alkyl thionitrites (RS−N═O), the analogous transition to a continuum results in dissociation dynamics typical of a repulsive dissociation with most of the excess energy appearing in the translational recoil of NO and its counterfragment and with very little in the vibration of the NO. We are therefore led to conclude from experiments, absorption properties, and expectations of the dissociation dynamics based on chemical analogy that the 355 nm one-photon photolysis of jet-cooled N_2O_3 and N_2O_4 does not contribute significantly to the observed NO($v'' = 2$) formation.

Figure 6 shows a typical rotationally resolved LIF excitation spectrum of the nascent NO($v'' = 2$) photofragment from the 355 nm photodissociation of jet-cooled HONO. Relative rovibronic LIF intensities were measured from the observed saturated spectra and evaluated by taking constant rotational line strengths. Owing to unfavorable signal-to-noise the rotational population distribution of nascent NO($v'' = 2$) was obtained by averaging data from several rotational branches. The distribution shown in Figure 7 is the average over both spin−orbit manifolds of NO and over several LIF scans recorded under similar experimental and identical conditions of production of the HONO parent.

The distribution displayed in Figure 7 is clearly bimodal with two distinctive peaks near $J = 5.5$ and $J = 25.5$, respectively. Computer simulation of the measured distribution reveals that it can be reproduced well by the sum (solid line in Figure 7) of a Boltzmann and a Gaussian distribution (dashed lines). The Boltzmann component peaks around $J = 5.5$ with a half width

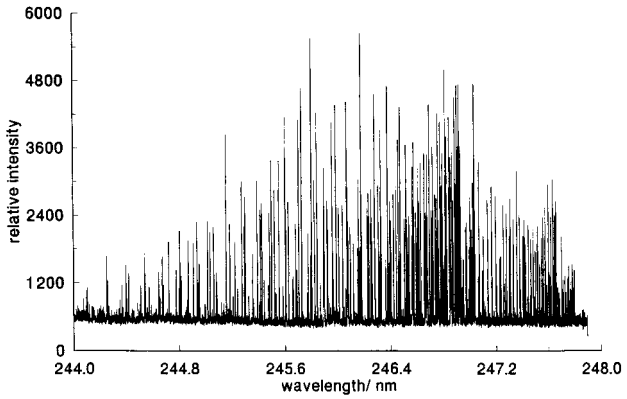

Figure 6. LIF excitation spectrum of NO ($v'' = 2$) photofragment on the $\gamma(0,2)$ band from the 355 nm photodissociation of jet-cooled HONO and HONO−water clusters.

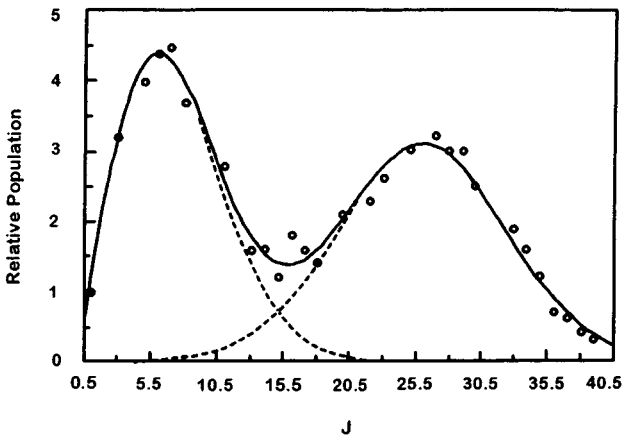

Figure 7. Rotational distribution of the NO($v'' = 2$) fragment deduced from LIF excitation spectra, such as the example shown in Figure 7. The solid line is the sum of a Gaussian and a Boltzmann distribution (dashed lines). The Gaussian and Boltzmann components are attributed to nacent NO from the photodissociation of HONO and HONO−H_2O clusters, respectively.

of 9.5, and the Gaussian component reveals a maximum at $J =$ 25.5 with a half width of 15. The Gaussian component of our NO distribution is thus in very good agreement with that measured by Dixon and Rieley for bare HONO[8] and in satisfactory agreement with distributions predicted by theory.[24] It can be attributed with confidence to the photodissociation of the jet-cooled bare HONO molecule. The Boltzmann component used in the simulated rotational distribution of Figure 7 was calculated for a rotational temperature of 170 K. We attribute this part of the distribution to NO($v'' = 2$) fragments from the photodissociation of HONO−H_2O complexes and small HONO−water clusters.

Discussion

HONO and Cluster Generation Method. The method chosen for HONO vapor production is suitable for the continuous generation of this compound at mixing ratios between 1000 and 10 000 ppm. Its main limitation remains, however, the well-known instability of HONO toward homogeneous and surface-induced decomposition and the consequent presence of significant amounts of NO and NO_2 . The presence of excess water vapor is unavoidable and, in fact, desirable for the production of HONO−water clusters. Continuous flow techniques suitable for the preparation of anhydrous gaseous HONO are not known. The method developed here relies on the rapid reaction of aqueous nitrite with acid and a slower, rate-determining transfer of HONO from the aqueous into the gas phase. It is complicated by the temperature-dependent decomposition of the acid in the liquid phase and the further slow decomposition in the gas phase according to

$$2\mathrm{HONO} \rightarrow \mathrm{NO} + \mathrm{NO_2} + \mathrm{H_2O} \qquad (6)$$

Reaction 6 and the reverse reaction as well as other HONO-producing reactions of the NO_x−H_2O system are known to be surface-catalyzed and relatively slow in the homogeneous gas phase.[1, 21,25,26] The partitioning of HONO among liquid, vapor, and adsorbed phases and competing liquid phase and surface-induced reactions lead to the observed complex but on the whole slight dependence of HONO yields on the reaction temperature.

Cluster formation has been mentioned previously as a complication in the jet-cooling of HONO for photodissociation studies.[8−12] The complex composition of samples and lack of any attempts to identify the main components may have discouraged further work on HONO clusters. The samples used in the present work consisted of the carrier gas and four relevant components in the proportion summarized in eq 4. Cluster formation between all these components and the very minor constituents N_2O and HNO_3 is possible in principle. An experimental technique, such as VUV photoionization and mass spectrometry of the resulting ions, is needed to aid the characterization of species distribution at the specific site of the jet probed by photofragment LIF. In the absence of such measurements we have to rely on predictions based on sample composition, expansion conditions, and chemical intuition concerning cluster formation tendencies.

If the tendency for formation of binary HONO complexes is equal for all components, relative abundancies of binary clusters formed in the jet will be proportional to the relative binary collision frequencies and hence to the product of individual number densities. This leads to a prediction of 1180:26:1:0.2:0.2 for the relative abundance of the clusters HONO−Ar:HONO−H_2O:$(HONO)_2$:HONO−NO_2:HONO−NO. All five species have the HONO chromophore albeit perturbed by complexation and will have similar absorption spectra shifted to a varying extent by complexation. All may produce vibrationally excited NO by photodissociation of HONO.

Signal-to-noise considerations indicate that a minimum mixing ratio of 200 ppm is required for HONO prior to expansion in order to produce a measureable photofragment LIF signal for the hot NO daughter fragment. HONO−NO_2 and HONO−NO are therefore not likely to make significant contributions to the observed LIF signal. Of the remaining three binary species dipole−dipole forces and H-bonding will lead to stronger attractive interaction forces between HONO and water molecules. These qualitative considerations indicate that the tendency for formation of HONO complexes with Ar is probably orders of magnitude lower than that of HONO with water. We therefore anticipate that the main clusters in our jet are the hydrogen-bonded dimer HONO−H_2O and its higher complexes with water of the type HONO$(H_2O)_n$. The dimer $(HONO)_2$ and the mixed clusters of the type $(HONO)_2(H_2O)_n$ may also be present. The relatively mild expansion conditions and small mole fractions involved with H_2O in roughly 10-fold excess argue for the binary complex HONO−H_2O and small HONO-$(H_2O)_n$ clusters as the prevailing species.

Photodissociation of Cold HONO. The structured $S_1(n,\pi^*) \leftarrow S_0$ electronic absorption spectrum and the dissociation dynamics of bare HONO on excitation at several wavelengths are already known in some detail from LIF measurements of the nascent OH and NO fragments.[7−11] Sophisticated experimental and theoretical studies have shown that the absorption

of near-UV photons in this spectral region results in dissociation according to eq 1 via a relatively long-lived excited state.[8,24] In the electronic ground state HONO occurs in two rotameric forms separated by a large internal rotation barrier, a more stable and abundant *anti* rotamer and an energetically disfavored *syn* conformer that is less stable by 2.7 kJ mol^{-1}. The equilibrium constant at 277 K has been determined as

$$K = N_{anti}/N_{syn} = 3.25 \quad (7)$$

by Bongartz et al.[16] The presence of two distinct conformers with slightly shifted electronic spectra gives rise to an overlapped, composite electronic absorption in the near-UV that is dominated at 300 K by the *anti* conformer. The characteristic vibronic features forming progressions in the N═O stretching mode of the Ã states of each conformer are interpreted as transitions to quasi-bound levels supported by a shallow well along the O−N dissociation coordinate. Alternatively, they may be described as short-lived resonances decaying by the dissociation of the weak, central O−N bond. The lifetimes of these levels appear to *increase* with n^*, the number of quanta in the N═O stretching vibration of the excited state, and hence, with transition energy as judged from the *decrease* in their spectral widths.[24] Excitation of these resonances can lead to vibrational adiabatic dissociation with retention of the vibration of the N═O fragment and to dissociation by conversion of N═O vibrational motion on the excited-state surface into translation along the dissociation coordinate. Excitation at 355 nm coincides with the 2^2_0 or $n^* = 2$ resonance of the prevailing *anti* rotamer with two quanta in the N═O stretching vibration of the excited state. The vibrational distribution of the NO fragment from the photolysis of 300 K HONO on this band has been measured by Dixon and Rieley and may be compared with distributions calculated by Henning et al.[27] and Cotting and Huber.[24] Both experiment and theory indicate that the $n^* = 2$ resonance decays preferentially by the nonadiabatic route with loss of one vibrational quantum:

$$HO{-}N{=}O(\tilde{A}\,^1A'' \; n^* = 2) \rightarrow HO(X^2\Pi) + N{=}O(^2\Pi\,, v'' = 1) \quad (8)$$

Our measurements relate to excitation of the $n^* = 2$ resonance of jet-cooled HONO and to the adiabatic channel leading to NO($v'' = 2$). No attempt was made to measure the ($v'' = 2$)/($v'' = 1$) vibrational ratio of the nascent NO because of interference from NO($v'' = 1$) from the photodissociation of NO_2.

The rotational distribution for NO($v'' = 2$) we have deduced ($J_{max} = 25$; fwhm, $\Delta J = 15$) is Gaussian in shape and is in good agreement with the previous ambient temperature measurement of Dixon and Rieley[8] who described their distributions as approximately Gaussian in J with a maximum around $J = 25.9$ and a half width of 15.2 for the $v'' = 2$ distribution. The distributions predicted for this channel by theory on the basis of a quasi-triatomic model are narrower and shifted to lower or higher J depending on the excited-state potential used.[24,28] The calculated distribution for the NO($v'' = 1$) channel in the dissociation of the $n^* = 2$ resonance has a pronounced minimum. We were unable to measure the NO($v'' = 1$) rotational distribution because of strong interference from the photodissociation of NO_2.[20,22] Our measurements indicate, however, that the width of the NO($v'' = 2$) rotational distribution does not appear to be narrowed significantly by jet-cooling the parent with Ar. This supports the notion that the angular momentum disposal observed in the 355 nm photodissociation of HONO is not described perfectly by the theory. Alternatively, cluster photodissociation makes a significant contribution to the production of rotationlly hot NO($v'' = 2$). These two alternatives can be distinguished in principle by measurements of the NO alignment. A substantial reduction in the alignment $A^{(2)}_0$ of NO($v'' = 2$) from the limiting value of +0.8 to +0.27 has been reported for the 355 nm dissociation of HONO at ambient temperature, but this may also be attributed to overall rotation of the parent during the lifetime of the excited molecule.[8,24]

Photodissociation of HONO Clusters. The low J part of the NO($v'' = 2$) photofragment rotational distribution clearly has a dynamical origin very different from the Gaussian component. Shifts in the rotational distribution of photofragments toward much lower angular momenta have been observed before on clustering of molecules and can be explained by channeling excess energy and momenta into additional degrees of freedom associated with cluster coordinates.[4−6] Less energy and smaller fractions of the phase space will be available for partitioning energy and angular momentum into the photofragments. The photodissociation of bare HONO and its alkyl derivatives gives rise to highly rotationally inverted NO. Complexation on jet-cooling can therefore be identified readily by the production of NO in low angular momentum states as noted previously for *tert*-butyl nitrite.[29] Kades et al. have recently studied the production of vibrationally excited NO in the near-UV photodissociation of CH_3ONO and $(CH_3)_3CONO$ clusters[30] and attributed the low J part of the observed bimodal rotational distributions to clusters of the type $[RONO]_n$ with a broad size distribution ranging from $n = 2$ to $n = 20$.[30]

We explain the Boltzmann-like component with $T_{rot} = 170$ K in our rotational distribution for NO($v'' = 2$) by the photodissociation of mixed HONO−water clusters. We have argued that the complexes HONO−H_2O and HONO$(H_2O)_n$ are likely to prevail as the precursor species but cannot of course exclude a broad cluster size distribution, although the observed significant retention of the vibrational excitation of NO by complexed HONO on excitation of the 2^2_0 feature at 355 nm indicates that the *anti*-HONO chromophore is not disturbed significantly by cluster formation. Significant hydration of HONO will shift the absorption spectrum of HONO to the blue in the direction of the broadened spectrum of the aqueous acid. A blue shift on complexation with water will favor excitation of lower quanta in the excited state at 355 nm.. Furthermore, vibrational relaxation during expulsion of the NO fragment from larger clusters is expected to reduce the yield of NO($v'' = 2$), whereas significant retention is observed. We therefore prefer the binary complex HONO−H_2O and small clusters of the type HONO$(H_2O)_n$ with $n = 2-5$ as the most likely parents of the observed rotationally cold NO($v'' = 2$) distribution. The vibrational state distribution of NO from the near-UV photodissociation of *tert*-butyl nitrite, where H-bonding in the clustered parent is unimportant, does not appear to be altered drastically by cluster formation. In that case some broadening of the high J Gaussian part of the rotational distribution of NO has also been observed but has been attributed to the photodissociation of the clustered parent molecules.[31]

Conclusions

We have developed a stable source for the continuous generation of gaseous HONO with high number density. The source has been used successfully for a study of photodissociation of bare HONO and of small HONO−H_2O clusters in a continuous supersonic jet expansion. Excitation of a mixture of jet-cooled *anti*-HONO and small HONO−water clusters on the 2^2_0 vibronic transition at 355 nm produces NO($v'' = 2$) with

a bimodal rotational distribution. The cold Boltzmann-like part of the distribution with T_{rot} of ca. 170 K has been explained by the photodissociation of the HONO−H_2O complex and of small HONO$(H_2O)_n$ clusters. The Gaussian shaped high J part of the photofragment distribution has been attributed to photolysis of bare *anti*-HONO and is in good agreement with the distribution previously measured for the 355 nm photolysis of 300 K HONO. The photodissociation of HONO−water complexes provides an interesting opportunity to reveal intricate dynamical details and may prove suitable for studying energy disposal into both OH and NO fragments, their vector attributes, and their relaxation in strongly H-bonded clusters. Further work using tunable photolysis, photofragment yield spectroscopy, and alignment measurements is necessary to quantify the influence of complexation of HONO with water on its dissociation dynamics.

Acknowledgment. This work was supported by a grant of the U.K. Engineering and Physical Sciences Research Council (EPSRC) and (in part) by a CEC contract (STEP CT 90-0071).

References and Notes

(1) Febo, A.; Perrino, C.; Gherardi, M.; Sparapani, R. *Environ. Sci. Technol.* **1995**, *29*, 2390.
(2) Zhang, R.; Leu, M. T.; Keyser, L. F. *J. Phys. Chem.* **1996**, *100*, 339.
(3) Shin, S. K.; Chen, Y.; Nicolaisen, S.; Sharpe, S. W.; Beaudet, R. A.; Wittig, C. *Adv. Photochem.* **1991**, *16*, 249.
(4) Sivakumar, N.; Hall, G. E.; Houston, P. L.; Hepburn, J. W.; Burak, I. *J. Chem. Phys*. **1988**, *88*, 3692.
(5) Zhang, J.; Dulligan, M.; Segall, J.; Wen, Y.; Wittig, C. *J. Phys. Chem.* **1995**, *99*, 13680.
(6) Fan, Y. B.; Donaldson, D. J. *J. Phys. Chem.* **1992**, *96*, 19.
(7) Vasudev, R.; Zare, R. N.; Dixon, R. N. *J. Chem. Phys.* **1984**, *80*, 4863.
(8) Dixon, R. N.; Rieley, H. *J. Chem. Phys*. **1989**, *91*, 2308.
(9) Shan, J. H.; Vorsa, V.; Wategaonkar, S. J.; Vasudev, R. *J. Chem. Phys.* **1989**, *50*, 5493.
(10) Shan, J. H.; Wategaonkar, S. J.; Vasudev, R. *Chem. Phys. Lett.* **1989,** *160*, 614.
(11) Novicki, S. W.; Vasudev, R. *J. Chem. Phys.* **1991**, *95*, 7269.
(12) Holland, S. M.; Stickland, R. J.; Ashfold, M. N. R.; Newnman, D. A.; Mills, I. M. *J. Chem. Soc., Faraday Trans.* **1991**, *87*, 3461.
(13) Cox, R. A. *J. Photochem*. **1974**, *3*, 175.
(14) Cox, R. A.; Derwent, R. G. *J. Photochem*. **1976**, *6*, 23.
(15) Kenner, R. D.; Rohrer, F.; Stuhl, F. *J. Phys. Chem*. **1986**, *90*, 2635.
(16) Bongartz, A.; Kames, J.; Welter, F.; Schurath, U. *J. Phys. Chem.* **1991**, *95*, 1076.
(17) Taira, M.; Kanda, Y. *Anal. Chem*. **1990**, *62*, 630.
(18) Braman, R. S.; de la Cantera, M. T. *Anal. Chem.* **1986**, *58*, 1533.
(19) McCoustra, M. R. S.; Pfab, J. *J. Chem. Soc., Faraday Trans.* 2 **1988**, *84*, 655.
(20) Ning, C.; Lin, H.; Pfab, J. *J. Phys. Chem*. **1993**, *97*, 7458.
(21) Wiesen, P.; Kleffmann, J.; Kurtenbach, R.; Becker, K. H. *Faraday Discuss.* **1995**, *100*, 121.
(22) Hunter, M.; Reid, S. A.; Robie, D. C.; Reisler, H. *J. Chem. Phys.* **1993**, *99*, 1093.
(23) Shaw, A. W.; Vosper, A. J. *J. Chem. Soc., Dalton Trans*. **1972**, 961.
(24) Cotting, R.; Huber, J. R. *J. Chem. Phys.* **1996**, *104*, 6208.
(25) Kaiser, E. W.; Wu, C. H. *J. Phys. Chem.* **1977**, *81*, 1701.
(26) Sakamaki, F.; Hatakeyama, S.; Akimoto, H. *Int. J. Chem. Kinet.* **1983**, *15*, 1013.
(27) Hennig, S.; Untch, A.; Schinke, R.; Nonella, M.; Huber, J. R. *Chem. Phys.* **1989**, *129*, 93.
(28) Schinke, R.; Untch, A.; Suter, H. U.; Huber, J. R. *J. Chem. Phys.* **1991**, *94*, 7929.
(29) Hippler, M.; Al-Janabi, F. A. H.; Pfab, J. *Chem. Phys. Lett.* **1992**, *192*, 173.
(30) Kades, E.; Rösslein, M.; Brühlmann, U.; Huber, J. R. *J. Phys. Chem.* **1993**, *97*, 989.
(31) Kades, E.; Rösslein, M.; Huber, J. R. *J. Phys. Chem.*, **1994**, *98*, 13556.
(32) Bass, A. M.; Ledford, A. E.; Laufer, A. H. *J. Res. Natl. Bur. Stand., Sect. A* **1976**, *80*, 143.